Distribution-based Level Set Segmentation for Brain MR Images

Jundong Liu[1], David Chelberg[1], Charles Smith[2], Hima Chebrolu[2]
[1]School of Elec. Engi. & Comp. Science
Ohio University, Athens, Ohio
[2]Department of Neurology
University of Kentucky, Lexington, KY

Abstract

In this paper, we propose a distribution-based active contour model for brain MRI segmentation. As a generalization of the Chan-Vese piecewise-constant model, our solution uses Bayesian a posterior probabilities as the driving forces for curve evolution. Distribution prior, if available, can be seamlessly integrated into the level set evolution procedure. Unlike other region-based active contour models, our solution relaxes the global piecewise-constant assumption, and uses locally varying Gaussians to better account for intensity inhomogeneity and local variations existing in many MR images. More accurate and robust segmentations are therefore achieved. Experiments conducted on synthetic and real brain MRIs demonstrate the improvement made by our model.

1 Introduction

Magnetic resonance imaging (MRI) is a rich source of information regarding the soft tissue anatomy of human brains. Segmentation of Magnetic resonance imaging (MRI) brain images into different tissue types, i.e., gray matter (GM), white matter (WM) and cerebrospinal fluid (CSF) is a critical and fundamental task for the large volume of 3D MRI data to be effectively utilized for disease diagnosis, functional analysis of brains and the treatment of disease related to brain anamolies.

A variety of approaches to brain MRI segmentation have been proposed in the literature. Histogram-based approaches estimate the probability of a class label given only the intensity for each voxel. Such estimation problems are usually formulated in the sense of maximum a posteriori (MAP) or maximum likelihood (ML) estimates. With respect to the form of the probability density function, finite Gaussian mixture models [12] are assumed and used in segmentation.

Recently, segmentation algorithms [15, 2, 3, 10, 13, 5] that use region-based active contour models have gained great popularity. Active contour without edge model, commonly known as Chan-Vese piecewise-constant model [2], uses a stopping term based on Mumford-Shah segmentation functional so that the model can detect object boundaries with or without gradient. Although impressive experimental results have been reported for this model and its variants [10, 5] some common drawbacks and limitations exist within this group of solutions. A *mixture of global Gaussians* (piecewise-constant can

be regarded as the degenerate case) has been used a convenient assumption for modeling the intensity distribution. *Global means* are utilized to discriminate regions from each other. However, "homogenous regions with distinct means" is rarely an accurate account in practice, especially for medical images. In addition, spatial distribution priors, often available and being used extensively in histogram-based models, are normally neglected in the region-based active contour models. Prior knowledge about the organ's location sometimes is an indispensable resource to separate certain tissue types from their surroundings.

Non-parametric region-based active contours models (Chan-Vese [3] and Tsai-Yezzi [13]) can theoretically handle the local intensity variation problem. In their algorithms, an image u_0 is modeled by piecewise smooth functions u^+, u^- that are defined inside and outside a closed active contour, respectively. The curve evolution is carried out through an iterative process. In each iteration, u^+ and u^- are estimated first, by solving a Poisson equation with Neumann boundary condition. Then, the level set function is updated following a gradient flow that minimizes the simplified Mumford-Shah functional. Unlike in the parametric models, images in the piecewise smooth framework (both Chan-Vese and Tsai-Yezzi) are modeled as a smooth random field within each region. Intensity variability thus can be handled across regions without the need to specify the change on statistical parameters.

However, with the burden to solve a Poisson PDE in each iteration, piecewise-smooth models suffer from inevitable high computational costs induced from solving certain huge sparse linear system. Being computationally expensive has been a major obstacle for these models to be used in practical 3D medical applications [8].

1.1 Our proposed solution

Aiming to reap the benefits and avoid the drawbacks of the piecewise-constant and piecewise-smooth models, we propose a bridging solution in this paper. To generalize the Chan-Vese model, we adopt Bayesian a posterior probabilities as the driving force for the curve evolution. Our model has two desired properties: 1) distribution prior can be seamlessly integrated into the level set evolution procedure and leads to more robust segmentations; 2) piecewise constant assumption is relaxed from "global" to "local", and *local means* are used as the area representatives. Being able to better account for intensity inhomogeneity, our model works particularly well for the images with low intensity contrasts and spatially varying brightness variations. When the computation switches from global to local, segmentation "twisting" (same objects are labeled oppositely at different local areas) may happen if no global control is in place. We tackle this issue with a selective update scheme, which enforces a global-to-local consistency over the entire image domain.

2 Methods

Let C be an evolving curve in Ω. C_{in} denotes the region enclosed by C and C_{out} denotes the region outside of C. Chan-Vese (two-phase) piecewise-constant model is to minimize the energy functional

$$F(c_1,c_2,C) \quad = \quad \mu \cdot \text{Length}(C) + \lambda_1 \int_{C_{in}} |u_0 - c_1|^2 dxdy + \lambda_2 \int_{C_{out}} |u_0 - c_2|^2 dxdy$$

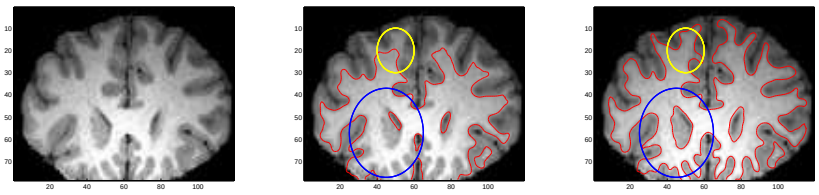

(a) (b) (c)

Figure 1: Chan-Vese model's inability to handle local image variations. a) is a slice of brain MRI image before bias correction. b) is the curve evolution result using Chan-Vese model. c) is the result using our method.

where c_1 and c_2 are the averages of u_0 inside C and outside C respectively.

This model has several attractive properties: 1) it is very robust to weak boundaries and noise; 2) interior contours can be automatically recovered; 3) the initial curve can be anywhere in the image; 4) it has few parameters for adjustment compared to MRF-based methods; 5) Efficiency wise, re-initialization of the level set function often is not required, and big step size can usually be taken for level set update.

These appealing advantages, however, are not easily utilizable to the full extent in practice. Global Gaussian distribution assumption are not an accurate depiction of local image profile for many medical images. Negligence of local information would often result in undesired segmentations. Figure 1 shows an example where the Chan-Vese piecewise-constant model fails to produce an expected segmentation result. Fig 1.a) is an MR image with bias field. The bias field lights up gradually from the top to the bottom of the image. Due to this intensity variation, the global means c_1 and c_2 can not represent the image well, and undesired segmentation, as highlighted in Fig 1.b), is resulted. (The figure is better seen on screen than in print)

Piecewise-smooth models [3, 13] provide a solution for the intensity variability problem. Gradual intensity changes, as in the Fig. 1 can be handled with [3, 13], however, high computational cost and being sensitive to curve initialization pose a barrier for practical applications.

2.1 Our Local Distribution-based Model

Let $S = \{in, out\}$ be the two classes for a two-phase model. The probability of the pixel (x,y) belonging to *in* and *out* is denoted by $P(in|(x,y))$ and $P(out|(x,y))$ respectively. Let $Pr(in)$ and $Pr(out)$ be the class prior probabilities at (x,y). Then,

$$P(in|(x,y)) = \frac{Pr(in_{(x,y)})P(u_0(x,y)|in)}{P(B)} \quad P(out|(x,y)) = \frac{Pr(out_{(x,y)})P(u_0(x,y)|out)}{P(B)} \quad (1)$$

where $P(u_0(x,y)|in)$ is the likelihood of a voxel in class *in* has the intensity of $u_0(x,y)$. $P(B)$ is a constant. Bayesian decision rule states that $u_0(x,y)$ should be classified into the class *in* if:

$$Pr(in_{(x,y)})P(u_0(x,y)|in) > Pr(out_{(x,y)})P(u_0(x,y)|out)$$

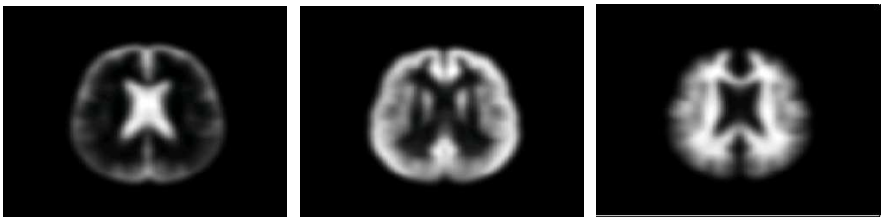

(a) (b) (c)

Figure 2: Spatial prior probability images of CSF, GM and WM.

or otherwise into *out*. If a perfect segmentation/classicition is achieved, this inequality should hold for each voxel (x,y), if every pixel has been classified into the correct class. Based on this observation, we can formulate the segmentation problem as the minimization of the following energy:

$$\begin{aligned} F(C) &= \mu \cdot \text{Length}(C) - \int_{C_{in}} \log(Pr(in)P(u_0(x,y)|in))dxdy \\ &\quad - \int_{C_{out}} \log(Pr(out)P(u_0(x,y)|in))dxdy \end{aligned}$$

Note that our overall model is similar to [10, 11], but the setup of the likelihood term is different, which will be explained next.

2.1.1 Spatial distribution priors: $Pr(in)$ and $Pr(out)$

Many distribution prior images have been generated from recent brain studies [4]. A widely used model is provided by the Montreal Neurological Institute [7] as part of the ICBM, NIH P-20 project. MNI prior is made of three probability images that contain values in the range of zero to one, representing the prior probability of a voxel being either GM, WM or CSF after an image has been normalized to the same space (see Figure 2). In this paper, we are particularly interested in extracting sub-cortical GM, therefore we take the GM and WM prior images as $Pr(in)$ and $Pr(out)$ respectively, for demonstration purpose. For these prior images to be applied, a registration is need to align the prior and the input image. We used the affine registration routine provided by SPM [12] in all the 3D experiments of this paper.

2.1.2 Likelihood terms: global Gaussian versus local

As illustrate in Fig. 1, global Gaussians and global means are not an accurate description of the local image profile, especially when intensity inhomogeneity is present. A remedy is to relax the global Gaussian mixture assumption and take local intensity variations into consideration. More specifically, local Gaussians (local binary as the degenerate case) should be used as a better approximation to model the vicinity of each voxel.

In the Chan-Vese model, two global means c_1 and c_2 are computed for C_{in} and C_{out}. In our approach, we introduce two functions $v_1(x,y)$ and $v_2(x,y)$, both defined on the image domain, to represent the mean values of the *local* pixels inside and outside the moving curve. By *Local*, we mean that only neighboring pixels will be considered. A simple

implementation of the "neighborhood" is to introduce a rectangular window $W(x,y)$ with size of $2k+1$ by $2k+1$, where k is a constant integer. Therefore,

$$v_1(x,y) = \text{mean}(u_0 \in (C_{in} \cap W(x,y)))$$
$$v_2(x,y) = \text{mean}(u_0 \in (C_{out} \cap W(x,y)))$$

With the new setup, our segmentation model can then be updated as a minimization of the following energy:

$$F(v_1,v_2,C) = \mu \cdot \text{Length}(C) - \int_{C_{in}} \left(\log(Pr(in)) - \log(\sigma_1) - \frac{(u_0-v_1)^2}{2\sigma_1^2} \right) dxdy - \int_{C_{out}} \left(\log(Pr(out)) - \log(\sigma_2) - \frac{(u_0-v_2)^2}{2\sigma_2^2} \right) dxdy$$

The variances σ_1 and σ_2 should also be defined and estimated locally. However, due to the fact that local variance estimation tends to be very unstable, we use global variances (for the pixels in C_{in} and C_{out}) as uniform approximation.

2.2 Level set framework and gradient flow

Using the Heaviside function H, and the one-dimensional Dirac measure δ [2] as the bridge, the energy function $F(v_1,v_2,C)$ can be minimized under the level set framework. Let $T_1 = \log(Pr(in))$ and $T_2 = \log(Pr(out))$, and we have the following new functional to minimize:

$$F(v_1,v_2,C) = \mu \int_\Omega \delta(\phi|\nabla\phi|)dxdy - \int_\Omega \left(T_1 - \log(\sigma_1) - \frac{(u_0-v_1)^2}{2\sigma_1^2} \right) H(\phi)dxdy - \int_\Omega \left(T_2 - \log(\sigma_2) - \frac{(u_0-v_2)^2}{2\sigma_2^2} \right) (1-H(\phi))dxdy$$

Under the level set framework, we deduce the associated Euler-Lagrange equation for the level set function ϕ. Parameterizing the descent direction by an artificial time $t \geq 0$, the gradient flow for $\phi(t,x,y)$ is given as

$$\frac{\partial\phi}{\partial t} = \delta(\phi) \left[\mu \text{div}\left(\frac{\nabla\phi}{|\nabla\phi|}\right) - \log\frac{Pr(in)}{Pr(out)} + \log\frac{\sigma_1}{\sigma_2} - \left(\frac{(u_0-v_1)^2}{2\sigma_1^2} - \frac{(u_0-v_2)^2}{2\sigma_2^2} \right) \right] \quad (2)$$
$$\phi(0,x,y) = \phi_0(x,y) \text{ in } \Omega$$

where ϕ_0 is the level set function of the initial contour. This gradient flow is the evolution equation of the level set function of our proposed method.

Correspondingly, v_1 and v_2 are computed with

$$v_1 = \frac{(u_0 * H(\phi)) \otimes W}{H(\phi) \otimes W} \qquad v_2 = \frac{(u_0 * (1-H(\phi))) \otimes W}{(1-H(\phi)) \otimes W} \quad (3)$$

where $\otimes$ is the convolution operator. One should note that, Chan-Vese model can be regarded as a special case of our model — when the window W is set to infinitely large.

In practice, the Heaviside function H and Dirac function δ in eqn. 3 have to be approximated by smoothed versions. We adopt the $H_{2,\varepsilon}$ and $\delta_{2,\varepsilon}$ used in [2]. For all the experiments conducted in this paper, we set the size of the window W as 21×21.

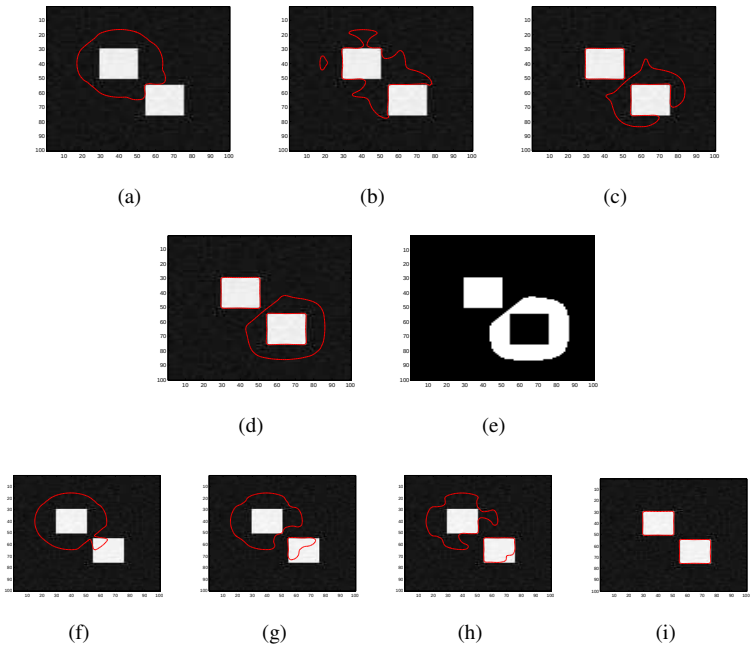

Figure 3: Illustration of the occurrence of "local twists". a), b), c) and d) are four snapshots of the level set propagation. e) is the resulted segmentation. The effectiveness of the control term is illustrated in (f-i), which are four snapshot of the level set propagation of the new gradient flow. (The figures are better seen on screen than in black-white print)

3 Global-to-Local Consistency Constraint

In Chan-Vese piecewise-constant model, as the entire image is considered as a whole, the signs of the level set function ϕ correspond very well to the segmented classes. In other words, if certain class S has more than one components, at the time a perfect segmentation is achieve, each of them would be enclosed at the same side of ϕ. The positive side (ϕ^+) and the negative (ϕ^-) side of ϕ, partition the image domain into two homogeneous regions.

However, under our proposed local Gaussian environment, this property is not guaranteed. Since the level set function ϕ evolves based on $v_1(x,y)$ and $v_2(x,y)$ that are computed locally, the multiple components of a same class might be evolved into the opposite sides of ϕ, therefore labeled with different classes. We give a name to this phenomena as *local twisting*. An example in Fig. 3 illustrates how a *twist* occurs. The evolving curve starts as a circle covering part of the left square. As v_1 and v_2 are computed locally, it happens that the left half the level set function ϕ goes up, and the right half goes down. Eventually the left square is enclosed under ϕ^+ and the right square under ϕ^-. The two squares are expected to classified into the same class, but the evolution based on Eqn.3 sends them into two different groups, as shown in Fig 3.b. The phenomenon is due to the lack of global control over the evolution process. Whenever *local twisting* happens, incorrect segmentation will be resulted.

Assume we use ϕ^+ to capture the brighter portion of a bimodal image. In order to eliminate *local twists*, the following consistency constraint needs to be enforced everywhere in the image domain:

Constraint: $v_1(x,y) \geq v_2(x,y)$**, for all** $(x,y) \in \Omega$

There would be many different implementations to enforce this constraint, and we find the following approach particularly effective and simple:

Solution: use sign$(v_1(x,y) - v_2(x,y))$ **as a control term to guide the update of** ϕ.

where $\text{sign}(x) = 1$, if $x > 0$ and $\text{sign}(x) = 0$ otherwise.

At the locations where no twist is present, $v_1 > v_2$, this control term $\text{sign}(v_1(x,y) - v_2(x,y))$ would let the level set update as Eqn.3 specifies. At certain locations, if $v_1(x,y) < v_2(x,y)$ happens, the control term put a halt to the level set update at (x,y), and further development of a potential twist is avoided. Through this mechanism, twists are controlled at an early stage, and will eventually disappear when the normal configuration $(v_1 > v_2)$ dominates over the image domain.

The above analysis, together with the solution, also applies to the case that we use ϕ^+ to capture the darker object. Putting the above analysis together, the updated gradient flow for our model is modified to:

$$\frac{\partial \phi}{\partial t} = \text{sign}(v_1 - v2) \cdot \delta(\phi) \left[\mu \text{div}(\frac{\nabla \phi}{|\nabla \phi|}) - \log \frac{Pr(in)}{Pr(out)} + \log \frac{\sigma_1}{\sigma_2} - \left(\frac{(u_0 - v_1)^2}{2\sigma_1^2} - \frac{(u_0 - v_2)^2}{2\sigma_2^2} \right) \right] \quad (4)$$

$$\phi(0,x,y) = \phi_0(x,y) \text{ in } \Omega$$

4 Results and Discussions

The fist experiment we conducted is based on the image shown in Fig 1.a. We tried to segment this 2D brain image into GM and WM. Since no prior information is available, we set $\log(Pr(in))$ and $\log(Pr(out))$ both to 0.5. Our result is shown in Fig 1.c, along with that of Chan-Vese model in Fig1.b. It is evident that our method can capture the local details, and produces a very accurate segmentation.

The second example is another MR image with bias field. Due the existing bias field, this image greatly violates the *global Gaussian/mean* assumption, therefore traditional region-based approaches, including the Chan-Vese model, are expected to fail. Figure 4 shows the result of using Chan-Vese model (left column) and that of using our local median model (right column). Three snapshots of the executions are provided. As evident, Chan-Vese model has trouble in capturing the GM area in the top-left and right-bottom corners, while our model separate the two issues very accurately.

The third experiment is based on the same MR image, but with an added artificial bias field. The result is shown in Fig 5. The purpose of the added field is to test how well our new model in handling severe intensity variation. Owing to the tremendous amount of inhomogeneity, piecewise-constant model totally failed, while our model still works very well without being affected by the bias level. This experiment also serves as a very good indication of the robustness of our approach.

The last group experiments were conducted on seven 3D MR images. All subjects are participants in the longitudinal University of Kentucky Alzheimer's Disease Center

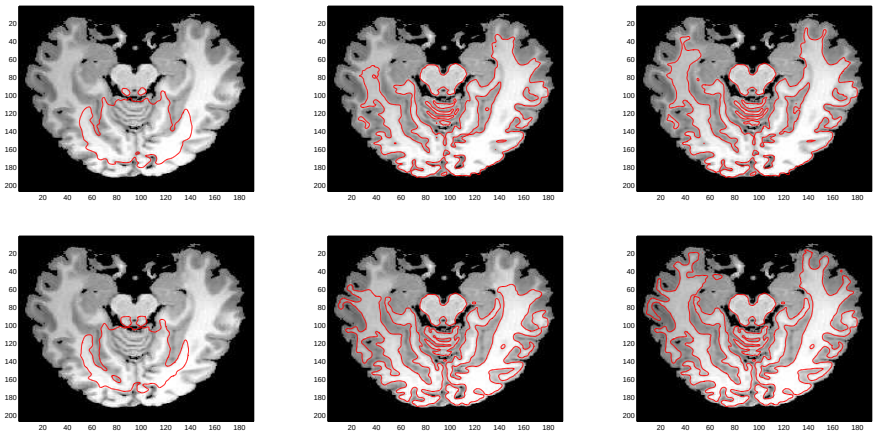

Figure 4: Segmentation comparison of Chan-Vese model and our model in handling bias field. First row: three snapshot of the execution on Chan-Vese model; Second row: three snapshot for our model. (The figures are better seen on screen than in print)

"biologically resilient adults in neurological studies" (BRAiNS) group. Scanning was performed on a Siemens Vision 1.5T instrument. We compared our solution with that of SPM [12] and Chan-Vese model. Fig. 6 shows a single slice result from all three methods. Fig.6.a is the input image, and 6.b, 6.c and 6.d are the GM segmentation from SPM, Chan-Vese and our model, respectively. The sub-cortical GM tissues in all the seven images have a bit higher intensity values than cortical GM, therefore the Chan-Vese model, using a piece-wise constant assumption, mis-classifies quite a portion of putamen as WM. Our model, on the other hand, clearly separates the putamen and thalamus from their surrounding WM. The comparison for the sub-cortical area has been highlighted with a red circle in Fig.6 (Figures are better seen on screen than in black-white print). Spatial distribution prior and local Gaussians both play a role in achieving this improvement. Compared to SPM, our model has the edge in outlining cleaner cortical GM (highlighted with a blue circle; better seen on the screen). Since level set methods all generate binary segmentations, our model can be used as a discrete alternative for SPM.

References

[1] K. V. Leemput et al., Automated model-based tissue classification of MR images of the brain", IEEE Trans. on Medical Imaging, vol. 18, pp. 897-908, 1999

[2] T. F. Chan and L. A. Vese, Active contours without edges, IEEE Trans. on Image Processing, Vol. 10, No. 2, pp. 266-277, 2001.

[3] T. F. Chan, L. A. Vese, A level set algorithm for minimizing the Mumford-Shah functional in image processing, 1st IEEE Workshop on Variational and Level Set Methods in Computer Vision, pages 161-168, 2001.

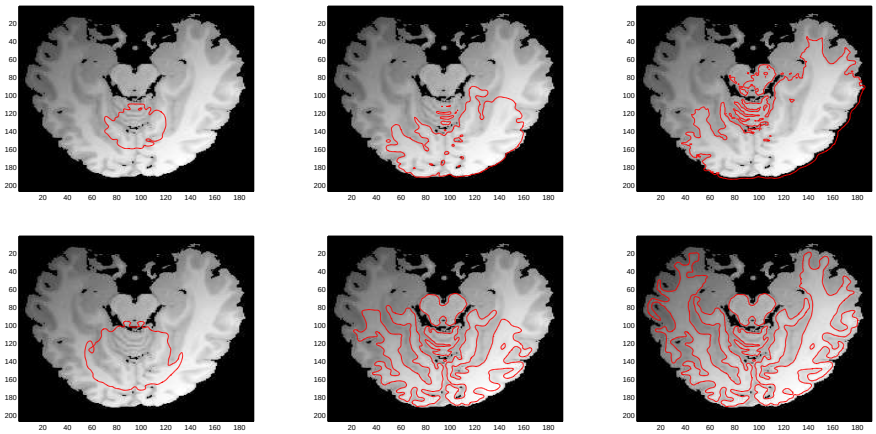

Figure 5: Segmentation comparison of Chan-Vese model and our model in handling severe intensity inhomogeneity. First row: three snapshot of the execution on Chan-Vese model; Second row: three snapshot for our model. (The figures are better seen on screen than in print)

[4] C. A. Cocosco et al., BrainWeb: Online interface to a 3D MRI simulated brain database, Neuroimage, vol. 5, no. 4, part 2/4 S245, 1997

[5] D. Cremers, M. Rousson and R. Deriche, "A review of statistical approaches to level set segmentation: integrating color, texture, motion and shape", IJCV, 2006. To appear.

[6] J. Yang, H. Tagare, L. H. Staib, J. S. Duncan, "Segmentation of 3D Deformable Objects with Level Set Based Prior Models". ISBI 2004: 85-88.

[7] A. C. Evans, D. L. Collins and B. Milner, "An MRI-based stereotactic atlas from 250 young normal subjects", Society of Neuroscience Abstrasts, 18:408, 1992.

[8] S. Gao, T. D. Bui, Image Segmentation and Selective Smoothing by Using Mumford-Shah Model. IEEE Transactions on Image Processing 14(10), 1537-1549, 2005.

[9] C. Li, J. Liu, M. D. Fox: Segmentation of Edge Preserving Gradient Vector Flow: An Approach Toward Automatically Initializing and Splitting of Snakes. CVPR (1) 2005: 162-167.

[10] N. Paragios and R. Deriche, "Coupled Geodesic Active Regions for Image Segmentation: A Level Set Approach", ECCV (2) 2000, pp. 224-240.

[11] M. Rousson, R. Deriche, "A Variational Framework for Active and Adaptative Segmentation of Vector Valued Images", INRIA Technical Report, 2002.

[12] A. Mechelli, C.J. Price, K.J. Friston, and J. Ashburner. "Voxel-Based Morphometry of the Human Brain: Methods and Applications". Current Medical Imaging Reviews, pp 105-113, 2005.

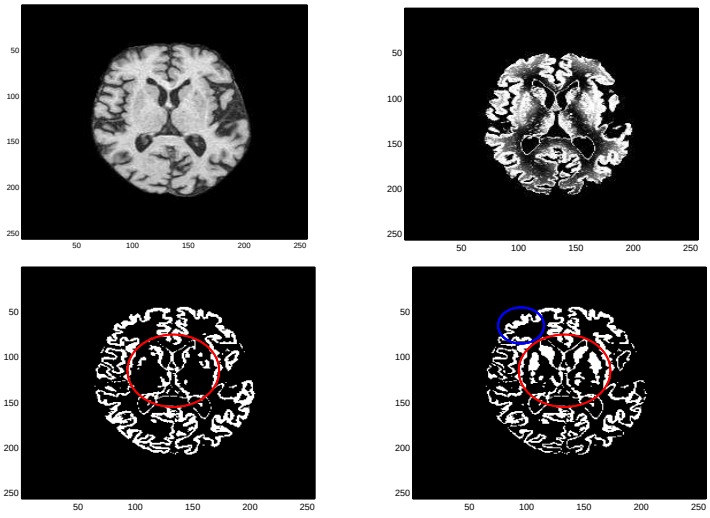

(c) (d)

Figure 6: Input image and 3 GM segmentation results from SPM (b), Chan-Vese (c) and our model (d).

[13] A. Tsai, A. Yezzi, W. Wells, C. Tempany, D. "Approach to Curve: Evolution for Segmentation of Medical Imagery", IEEE TMI, Vol. 22, No. 2, 137-154, February 2003

[14] C. Xu and J. L. Prince, "Snakes, Shapes, and Gradient Vector Flow," IEEE Transactions on Image Processing, 7(3), pp. 359-369, March 1998.

[15] S. Zhu and A. Yuille, "Region competition: Unifying snakes, region growing, and bayes/MDL for multiband image segmentation", PAMI, 18(9):884–900, 1996.